Permeation Properties of the Stereoregular Nylon-3 Analogue, Poly(α-hexyl β-L-aspartate)

Vicente Compañ,[†] David Zanuy,[‡] Andreu Andrio,[†] Marga Morillo,[‡] Carlos Alemán,[‡] and Sebastián Muñoz-Guerra*[,‡]

Departament de Ciencies Experimentals, Universitat Jaume I, 12080 Castellón, Spain, and Departament de'Enginyeria Química, Universitat Politécnica de Catalunya, ETSEIB, Diagonal 647, 08028 Barcelona, Spain

Received February 23, 2001; Revised Manuscript Received January 30, 2002

ABSTRACT: The permeabilities of thin films of the α-helix-like poly(β-peptide), poly(α-hexyl β-L-aspartate), to O_2, N_2, and CO_2 penetrants were measured by diffusion experiments at temperatures ranging between 20 and 80 °C. *P* and *D* coefficients were found to be higher for CO_2 than for the other two gases, and both parameters increased with temperatures for the three gases. Solubilities of N_2 and O_2 appeared to be independent of temperature whereas that of CO_2 decreased significantly upon heating. Solubilities of the three penetrants in the polypeptide were calculated by using advanced Monte Carlo methods specifically developed for the simulation of dense polymers. The structure of the polymer was modeled and optimized in a quasi-hexagonal lateral array of 13/4 helices with an average fixed interchain distance of 14.6 Å. Values predicted at low temperature were in satisfactory agreement with experimental data. At high temperatures significant discrepancies between the measured and calculated data were found for N_2 and O_2, which revealed the limitation of the Monte Carlo method to simulate the influence of temperature on the distribution of the unoccupied space.

Introduction

Poly(α-alkyl β-L-aspartate)s is a family of poly(β-peptide)s able to adopt regular folded arrangements similar to the well-known α-helix characteristics of poly(α-peptide)s and proteins.[1,2] These polymers may be also considered as nylon-3 analogues bearing an alkoxycarbonyl side group stereorregularly attached to the β carbon atom of the main chain:

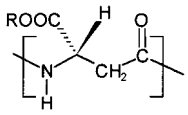

The structure of members with linear alkyl side groups, henceforth abbreviated PAALA-*n*, where *n* stands for the number of carbons contained in the alkyl group, has been systematically studied from methyl ($n = 1$) up to docosyl ($n = 22$).[1−5] The conformation preferred by these poly(β-peptide)s consists of a right-handed helix stabilized by intramolecular hydrogen bonds with 13 residues in four turns, i.e., the 13/4 helix. The length of the alkyl side group largely determines the type of arrangement adopted by the PAALA-*n* helices in the solid state. On one hand, PAALA-*n* with $n \leq 4$ tend to crystallize in a three-dimensional array of helices with the alkyl side groups forming part of the crystal lattice[2−4] (Figure 1a). On the other hand, comb-like PAALA-*n* with $n \geq 12$ form layered structures with main-chain helices and alkyl side chains distributed in two separate crystalline phases[5] (Figure 1b). PAALA-*n* with side chains of intermediate size, which are those with $n = 6$, 8, and 10, display a rather ambiguous behavior consistent with the structural discontinuity existing between short and long alkyl side chain polymers.[5,6] In fact, they tend to be arranged in a two-dimensional array of side-by-side packed helices with the alkyl chains remaining in the molten state and filling the interhelical space.

The structure of poly(α-hexyl β-L-aspartate), i.e., PAALA-6, has been examined by X-ray diffraction, solid-state NMR, and computer simulations.[5,6] X-ray diffraction of uniaxially oriented films of this polymer revealed the existence of an equatorial spacing at ∼1.7 Å that could be associated with the lateral dimension of a rough hexagonal array of 13/4 helices. CP-MAS ^{13}C NMR spectra recorded at temperatures between 25 and 80 °C were in accordance with the presence of the helical conformation along the whole interval of examined temperatures and did not show differences indicative of the occurrence of structural transitions upon heating. Furthermore, molecular mechanics calculations indicated that the hexyl side chains are unable to crystallize separately and also to pack efficiently in a tridimensional lattice.[6] As a result, the structure of PAALA-6 was envisaged as an approximate hexagonal packing of 13/4 helices lacking axial register and having the hexyl side chains in a disordered arrangement.

The solubility and transport of penetrant molecules in heterophasic polymers have become topics of interest in the past years. Thus, in semicrystalline polymers, the nature, amount, and distribution of the amorphous phase are known to be the factors determining largely the permeability of the material. Permeation properties have been investigated for a number of partially ordered polymers using both experimental and computational methods.[7−14] In this context, PAALA-*n* with medium or large values of *n* deserve particular attention since they form supramolecular structures composed of two well-delineated phases with completely different characteristics.[15] Since a different response to external stimuli may be expected for each phase, these systems open the door to the control of certain properties, which, like

[†] Universitat Jaume I.
[‡] Universitat Politécnica de Catalunya.
* Corresponding author: e-mail munoz@eq.upc.es.

10.1021/ma010321a CCC: $22.00
Published on Web 04/27/2002

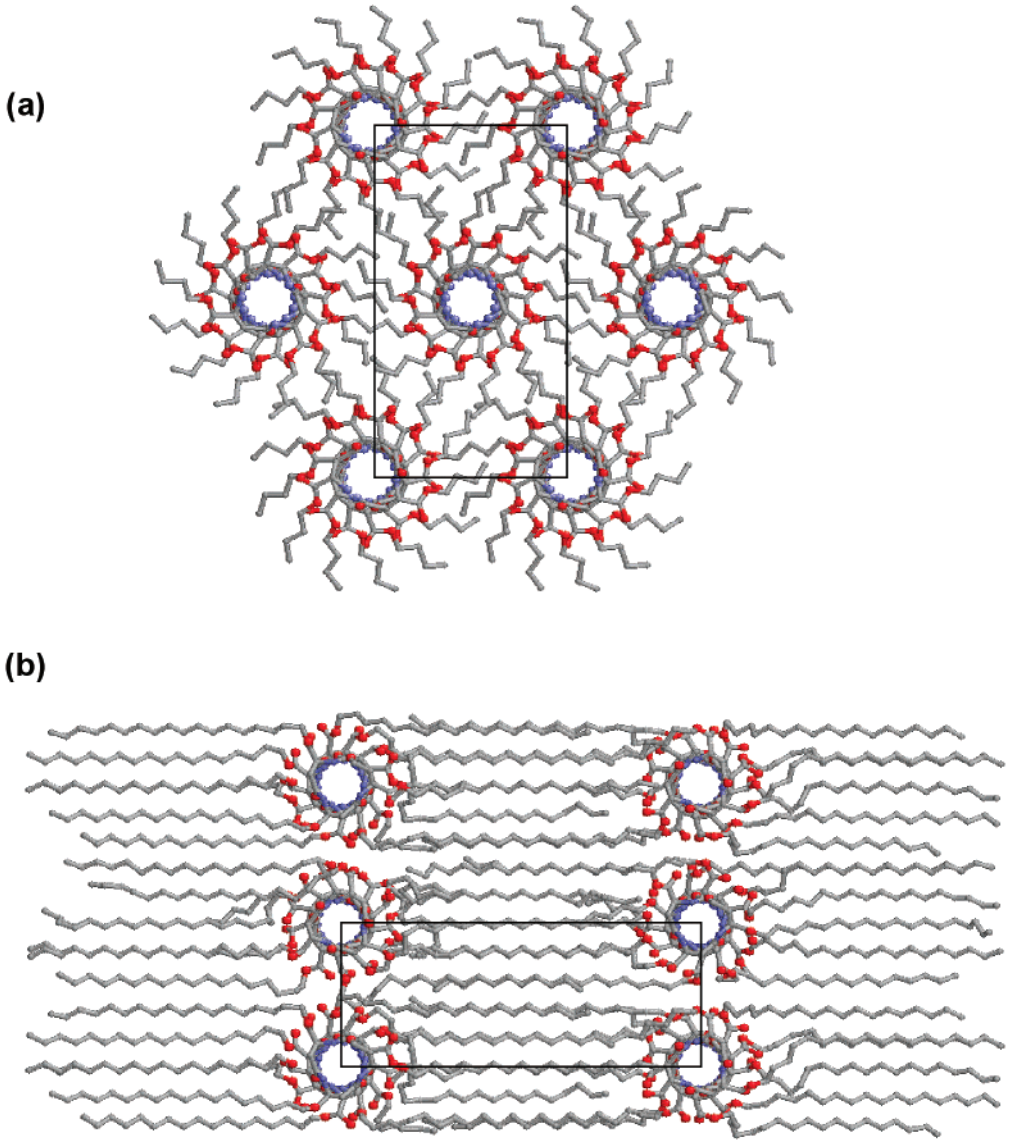

Figure 1. Schematic projections down the chain axis of PAALA-*n*: (a) the hexagonal crystal structure of PAALA-4; (b) the biphasic layered structure of PAALA-18.

permeability, depend on the microscopical structure and morphology of the material. However no experimental determination of gas transport in biphasic poly(*β*-peptide)s, or even in the more widely known comblike poly(α-peptide)s, has been performed so far. Recently, we have carried out some theoretical studies on the solubility of small molecules in polymeric matrices of PAALA-*n*. We specifically examined the solubility of gaseous penetrants in the crystal structures of PAALA-1 and PAALA-4[12] as well as in the layered structures of PAALA-*n* with $n \geq 12$.[13,14] Results obtained from these computational studies predicted that small penetrants are very soluble in the latter compounds but that a much lower solubility should be expected in PAALA-*n* with $n \leq 4$. On the contrary, no similar study on the behavior of PAALA-*n* bearing side chains of intermediate size has been carried out yet. The main objective of the present work is to evaluate the transport properties of simple penetrants in films of PAALA-6 and to correlate the observed behavior with the microscopic structure of the polymer. For this, the permeation coefficients of N_2, O_2, and CO_2 gases are first measured by membrane diffusion experiments, and then the solubilities of these penetrants in PAALA-6 are calculated by computational methods using the suitable simulated molecular structures.

Methods

A. Experimental Methods. 1. Materials and Intermediate Products. All chemicals were obtained commercially from either Aldrich or Merck. They were analytical grade or higher and used without further purification. Solvents to be used under anhydrous conditions were dried by standard methods. Poly(α-benzyl *β*-L-aspartate) (PABLA) was obtained by anionic ring-opening polymerization of 4(*S*)-4-benzyloxycarbonyl-2-azetidinone, as reported elsewhere.[16] This optically pure *β*-lactam was synthesized from natural L-aspartic acid by a well-established esterification−cyclation sequence of reactions.[17]

2. Polymer Synthesis. PAALA-6 was obtained by transesterification of PABLA with 1-hexanol in the presence of titanium tetrabutoxide, as is shown in Scheme 1. This procedure is of general validity for the preparation of PAALA-*n*, and a detailed account of the method will be published in the near future. In brief, a mixture of finely powdered PABLA and $Ti(OBu)_4$ suspended in an excess of 1-hexanol was heated at 180 °C and magnetically stirred under a nitrogen atmosphere. ^{1}H NMR analysis revealed that the replacement of the benzyl group by the hexyl group was complete after 25 min of

Scheme 1

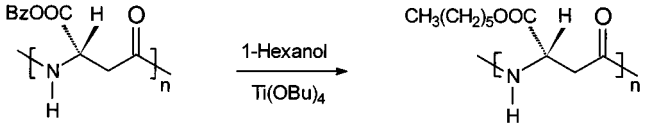

Table 1. Synthesis Data of PAALA-6

[PABLA]/[*n*-$C_6H_{11}OH$]	1/115
[PABLA]/[$Ti(OBu)_4$]	1/0.4
yield (%)	85
conv (%)[a]	100
[η] (dL g^{-1})[b]	2.62
M_v[c]	2.2×10^5
ρ (g mL^{-1})[d]	1.06

[a] Degree of replacement of benzyl by *n*-hexyl group as determined by ^1H NMR. [b] Intrinsic viscosity measured in dichloroacetic acid at 25 ± 0.1 °C. [c] Viscosity-average molecular weight estimated by using the Mark−Howink equation reported for poly(*γ*-methyl α-L-glutamate).[18] [d] Density of the polymer measured by flotation in KBr aqueous solution−water mixtures.

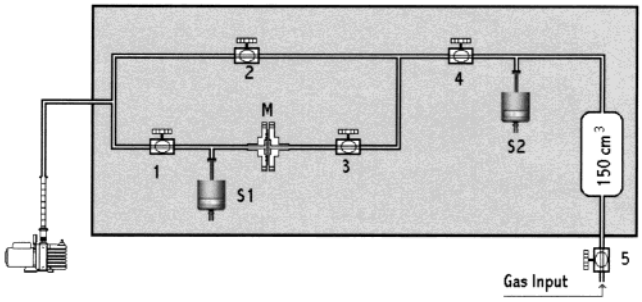

Figure 2. Experimental device used in the gas transport measurements.

treatment. The final reaction mixture solution was left to cool and then added with methanol to precipitate the alkylated polymer. PAALA-6 was recovered by filtration and repeatedly washed with methanol. For purification, the polymer was dissolved in chloroform containing a few drops of trifluoroacetic acid and then precipitated by addition of methanol. Synthesis data together with some of the most relevant characteristics of PAALA-6 are given in Table 1.

3. Permeation Measurements. PAALA-6 films to be used for permeation experiments with a thickness of approximately 150−200 μm were prepared by hot-pressing in a Specac accessory (CTFM-P/N 15620). The average thickness of the membrane was calculated from five measurements using an electronic micrometer Deltascope MP10 manufactured by Fischer. The thickness obtained was 190 ± 2 μm. Permeation measurements were carried out in the experimental device schematically represented in Figure 2. The apparatus consists of a cell with two chambers separated by the membrane, which is immersed in a computer-controlled thermostatic bath. Vacuum is made in both chambers by means of a vacuum pump model Trivac D 1,6 B from Leybold AG, which can reach 4×10^{-4} mbar. Pressures in the upstream and downstream chambers were measured with an accuracy of 0.15% of reading using capacitive sensors Leybold DI 2000 sensor (S1) and Tylan General CDHD45-11 sensor (S2), respectively. Nupro pneumatic electrovalves, model SS-4BK-1C, controlled by a computer program were used. This program also controls temperature, vacuum, and gas filling of the upstream chamber and calculates both permeability and diffusion coefficients using the pressured data of the chambers. The program automatically repeats this job for each temperature and pressure of the upstream chamber. Before measurements were performed, the system was vacuum calibrated by measuring the inlet of air into the downstream chamber. Keeping all the valves open except valve 5, high vacuum was made for 24 h in both chambers. Then valves 2 and 3 were closed, and valve 5 was opened, allowing the gas to fill a 150 mL deposit up to a pressure close to that used for the experiment. Then, valves 1 and 3 were suddenly opened and closed, respectively, and this time was taken as zero reference. The evolution of the pressure in the downstream chamber with time was monitored by the transducer pressure sensor CDHD45-11. The volume in the downstream chamber was measured by using the helium expansion technique. The value of this volume was fixed at 33.5 mL in order to get downstream pressures sufficiently low in relation to the pressure of the upstream chamber. In all experiments, the relation $p_l < 0.01p_0$ was satisfied. The permeation measurements were performed in the temperature range 20−80 °C, using steps of 10 °C for pressure differences of 0.5, 1, 2, 4, and 7 atm.

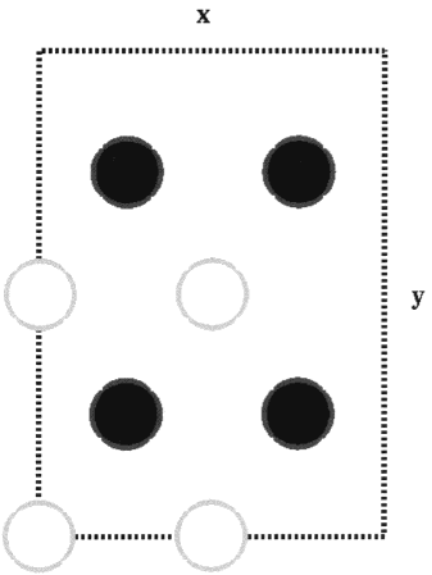

Figure 3. Schematic representation of the simulation box used for MC calculations of PAALA-6. The circles refer to the position of the eight chains explicitly included. Filled and empty circles correspond to chains pointing up and down, respectively.

B. Computational Methods. 1. Monte Carlo Simulations. The atomistic structure of PAALA-6 was reinvestigated using an advanced Monte Carlo (MC) sampling technique (Continuum Configurational Bias, CCB-MC).[19,20] This method has been recently adapted to the study of dense polymers with either partially or completely ordered structures. The method has been implemented into a computer program denoted MCDP (Monte Carlo simulations of Dense Polymers),[21] which has been optimized and parallelized to obtain a maximum computational efficiency. This strategy has been successfully used in the structural study of PAALA-*n* with $n = 8$, 12, 14, 16, and 18.[13,14,21] In addition to CCB moves, a small fraction of Metropolis moves (20%) were also used in all the simulations.

The box used in the simulations of PAALA-6 consists of eight independent chains arranged in antiparallel, as schematically represented in Figure 3. Periodic boundary continuation conditions and the minimum-image convention were applied to all simulations. The initial atomic coordinates were taken from our previous molecular mechanics study, in which an atomistic model was proposed for PAALA-6 on the basis of energy minimization calculations.[6] Such a model was compatible with the experimental information gained from solid-state NMR and X-ray diffraction data: (i) the chain backbone is in a right-handed 13/4 helical conformation, and (ii) the helices are packed in a quasi-hexagonal array lacking axial register. The torsion angles of the 13/4 helix were kept fixed at the following values: $\varphi = 146.2°$, $\xi = -59.8°$, and $\psi = 128.8°$. This agrees with the experimental observation that the helical conformation is retained in the solid at high temperatures[5] and also in solution.[22]

MC simulations of both *NPT* and *NVT* type, i.e., with and without varying the size of the box, were performed at

Table 2. Lennard-Jones Potential Parameters for the Penetrants

penetrant	R (Å)	ϵ (kcal/mol)
N_2[a]	1.850	0.1890
O_2[a]	1.790	0.2333
CO_2[b]	1.850	0.1200
C		
O	1.600	0.2000

[a] An spherical model was used to describe these penetrants. [b] Represented by a model including the all three atoms with a C═O bond length of 1.162 Å. Accordingly, the penetrant is viewed as an ellipsoid of dimensions $d_1 = 2(1.600 + 1.162) = 5.524$ Å and $d_2 = 3.70$ Å. Both d_1 and d_2 were used as criteria for the unoccupied volume calculations.

temperatures of 20C and 80 °C. All the *NVT* simulations were run at room temperature for a total of 7.5×10^5 steps, and the coordinates were saved every 2500 steps after 2.5×10^5 steps of equilibration. *NPT* simulations at 20 °C were stopped when both the energy and the cell parameters were equilibrated. Simulations at 80 °C were run for a total of 6×10^5 steps, the coordinates being saved every 2500 steps after 1×10^5 steps of equilibration. Accordingly, 200 microstructures were recorded and analyzed for each simulation of *NVT* type.

The AMBER force field[23] was used to represent the electrostatic, van der Waals, and torsional energies of the system. The CH, CH_2, and CH_3 groups were described considering a model of united atoms. Thus, the resulting system contains 1560 explicit atoms. The van der Waals energy was computed in the usual pairwise additive way using a Lennard-Jones 6−12 potential. Electrostatic charges were previously determined by fitting the molecular electrostatic potential derived from quantum mechanical calculations to the classical one.[6] Electrostatic interactions were evaluated using a standard Coulombic potential. Nonbonding interactions were truncated at 8 Å.

2. Measurement of the Unoccupied Space. The volume not occupied by the polymer chains was estimated by dividing the simulation box of every microstructure into a three-dimensional uniformly spaced grid. Then, a penetrant was centered in each node, and the distance to the nearest atom of the polymeric matrix was measured. If this distance was larger than the sum of the van der Waals radii of the penetrant and the polymer atom, the node was identified as unoccupied. Calculations were performed considering a spacing between consecutive nodes of 0.50 Å. The O_2 and N_2 penetrants were described as simple spheres; i.e., a single center representation was used for such gases, whereas a model including explicitly the three atoms was used to represent CO_2.[7] The dimensions estimated for the three penetrants are listed in Table 2.

3. Solubility Calculations. Solubility, S_0, gives the concentration of the gas in a volume element of the polymer that is in equilibrium with the outside gas at a given pressure. The determination of S_0 consists of calculating the interaction energy of the penetrant with the polymer in which it has been inserted at random. Such energy is used for obtaining the excess chemical potential (μ_{ex}), S_0 being related to μ_{ex} by the following equation:

$$S_0 = \exp(-\mu_{ex}/RT) \tag{1}$$

The relation between the calculated solubility, S_0, and the experimental solubility coefficient S, in units of cm^3 (STP) $(cm^3$ Pa$)^{-1}$, is written as[24]

$$S = (T_0/Tp_0)S_0 \tag{2}$$

where $T_0 = 273.15$ K, T is the temperature of measurement, and $p_0 = 1.013 \times 10^5$ Pa.

The infinite dilution μ_{ex} of a penetrant sorbed in PAALA-6 was estimated using the Widom's test particle insertion method.[25] In this method the chemical potential of species i in a frozen N-particle system relative to an ideal gas mixture is related to the potential energy of inserting a test particle into the system at randomly chosen positions. The expression of μ_{ex} is

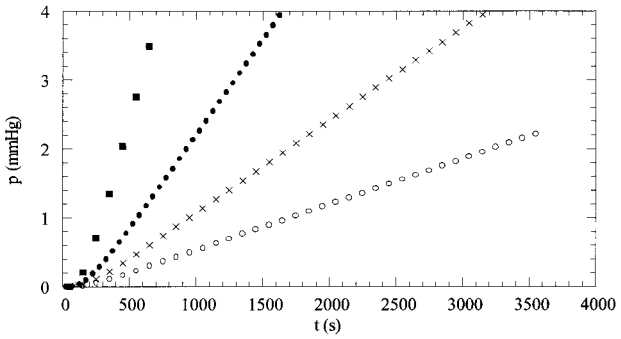

Figure 4. Variation of the pressure of carbon dioxide in the downstream chamber with time in PAALA-6 films. $p_0 = 0.5$ (○), 1 (×), 2 (●), and 7 atm (■).

$$\beta\mu_{ex}(\rho,T) = -\ln \langle \exp(-\beta\phi_t) \rangle_N \tag{3}$$

where $\beta = 1/k_bT$, ϕ_t is the interaction energy between the test particle and the N particles of the system, and $\mu_{ex}(\rho,T)$ is the excess chemical potential of species i at temperature T and number density $\rho = N/V$. The brackets $\langle ... \rangle_N$ denote the canonical ensemble average over the original N-particle system at the T and ρ of interest. To improve the insertion efficiency, the ensemble average $\langle \exp(-\beta\phi_t) \rangle_N$ has been defined as follows:

$$\langle \exp(-\beta\phi_t)_N \rangle = \sum_{j=1,N_e}(1/N_{T,j}) \sum_{i=1,N_{v,j}} \exp(-\beta\phi_{t,i}) \tag{4}$$

where $N_{v,j}$ is the number of sites without overlaps in the microstructure j, $N_{T,j}$ is the total number of insertions for a given microstructure j assuming a uniform insertion density, and N_e is the total number of microstructures available for computing the ensemble of averages.

To evaluate eq 4, the penetrant was centered at each node identified as unoccupied. Interactions between the penetrants and the polymer were computed using the Lennard-Jones 6−12 potential and applying the Lorenz−Berthelot mixing rules. Such interactions were truncated at 8 Å. The force-field parameters for the different penetrants considered in this study are displayed in Table 2.

Results and Discussion

Permeation Measurements. The transport of gases through membranes is generally expressed in terms of the apparent permeability coefficient P and the apparent diffusion coefficient D. Illustrative plots showing the variation of the CO_2 pressure in the downstream chamber with time at 25 °C and different pressures in the upstream chamber are represented for PAALA-6 in Figure 4. As usual, the curves present a transient state at short times followed by steady-state transport conditions at longer times. The intercept of the extrapolated steady part of the curve with the time axis gives the time-lag θ. This parameter is related to the apparent diffusion coefficient as indicated by Barrer,[26]

$$D = \frac{L^2}{6\theta} \tag{5}$$

where L is the thickness of the film. Under conditions of steady-state permeation, the apparent permeability can be evaluated by means of the following expression:[27]

$$P = \frac{273}{76} \frac{VL}{ATp_0} \frac{dp(t)}{dt} \tag{6}$$

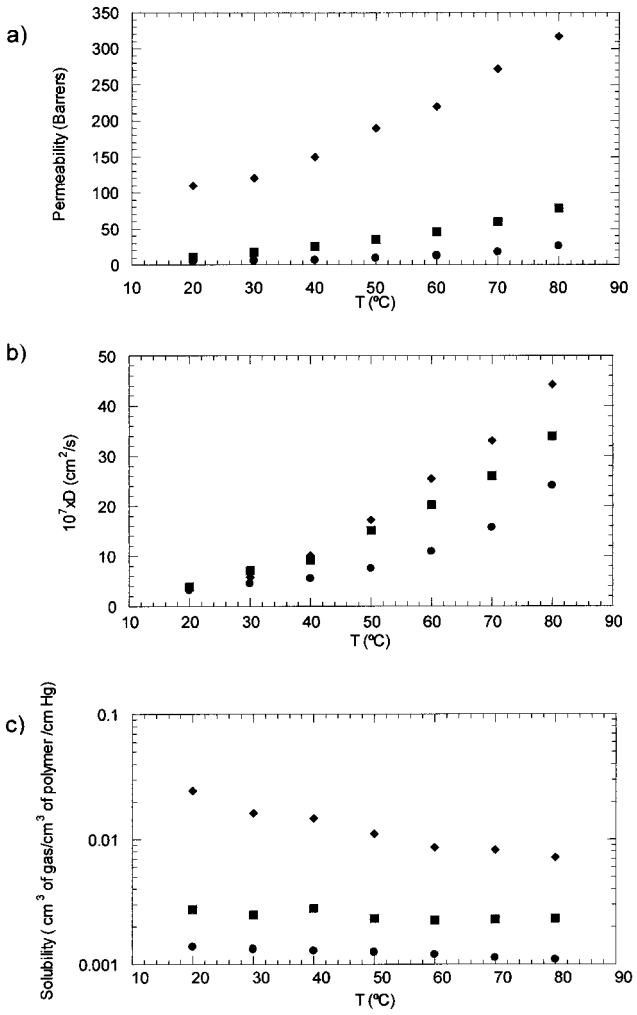

Figure 5. Temperature dependence of the apparent permeability (a), diffusion (b), and solubility (c) coefficients of CO_2 (◆), O_2 (■), and N_2 (●) through PAALA-6 films at $p_0 = 1$ atm.

where V and $p(t)$ are the volume and pressure of the downstream chamber, respectively, A is the effective area of the film, p_0 is the pressure in cmHg of the penetrant gas in the upstream chamber, and T is the absolute temperature. P is usually expressed in barrers (1 barrer $= 10^{-10}$ cm^3 (STP) of gas cm cm^{-2} s^{-1} $cmHg^{-1}$). P and D were found to be quite well reproducible so that the standard deviations for three consecutive measurements were ±2% and ±10%, respectively.

The dependence of the permeability coefficient of O_2, N_2, and CO_2, with temperature through PAALA-6 films, at $p_0 = 1$ atm, is represented in Figure 5a. Similar plots have been obtained for other pressures. This figure shows clearly that the permeability coefficient of the gases decreases in the following order $P(CO_2) > P(O_2) > P(N_2)$ at any temperature, the former being much larger than the other two. These results are in accordance with the general trend observed for other polymers.[28] The temperature dependence of the diffusion coefficient of O_2, N_2, and CO_2 are shown in Figure 5b. As expected, D increases steadily with temperature and shows the same relative order as the permeability coefficient with $D(CO_2) > D(O_2) > D(N_2)$. Contrary to what occurs in other many systems, the value of the apparent diffusion coefficient of N_2, O_2, and CO_2, in PAALA-6 films at low temperatures are very close to each other. This is also in contrast to the behavior observed for the permeability coefficient, which appears to be significantly larger for CO_2 than for O_2 and N_2. Comparison of results plotted in Figure 5a,b suggests that the enhanced permeability displayed by CO_2 with respect to O_2 and N_2 is due to its enhanced solubility in the membrane.

The apparent solubility coefficient S defined as

$$S = \frac{P}{D} \tag{7}$$

was calculated for the three gases at $p = 1$ atm, and the resulting values are plotted in Figure 5c for the considered interval of temperatures. It is seen that they follow the same relative order as the permeability and diffusion coefficients, i.e., $S(CO_2) > S(O_2) > S(N_2)$, but showing larger differences between them. The solubility of the three gases in the films decreases when the temperature increases, but the variation is much smaller for $S(N_2)$ and $S(O_2)$. Whereas at 20 °C these coefficients are about 20 and 10 times smaller than that of CO_2, at 80 °C such ratios are reduced to one-sixth and one-third, respectively. The results obtained with PAALA-6 films for the three gases show a logical correspondence between the permeation properties of the polymer and the physical characteristics of the diffusing molecule, being apparent that the permeability and the diffusion and solubility coefficients decrease as the kinetic diameter of the diffusing molecule increases. These tendencies are in accordance with the general behavior observed for other polymers.[29]

The effect of the pressure in the upstream chamber on the permeation properties of PAALA-6 films to O_2, N_2, and CO_2 at 25 °C for pressures up to 7 atm is depicted in Figure 6. The isotherms representing the variation of P, D, and S show the same pattern of behavior for the three gases. Whereas permeability P appears to be unaffected by the pressure (Figure 6a) within the whole range of pressures, the diffusion coefficient D (Figure 6b) exhibits an anomalous decrease in the low-pressure region, the upturn being the largest for N_2, intermediate for O_2, and smaller for CO_2. This behavior is opposite to that generally observed in semicrystalline polymers, where both the apparent permeability and the diffusion coefficient increase when the pressure decreases.[27,30] It should be noted also that the response of the diffusion coefficient to pressure variations is opposite to that given to temperature, which results in an interchange in the relative values of P and D for O_2 and CO_2. These results indicate that there is not apparent correlation between the permeability, the diffusion coefficient, and the physical characteristics of the diffusing molecule.

On the other hand, the solubility coefficient shows a small increase or upturn with decreasing values of p_0 in the low-pressure region for the three gases, with features similar to those observed for the $D-p_0$ isotherms (Figure 6c). It is clearly concluded from experimentation that the more condensable is the gas, the more soluble is it in the membrane. In other words, the relatively high boiling point of CO_2 should be responsible for the high solubility of this gas in PAALA-*n* in comparison with that of N_2 and O_2. The anomalous dependence of the transport properties on the upstream pressure suggests that the apparent solubility shown by the gases in PAALA-6 films could be the result of some structural changes taking place in the polymer by thermal or pressure effects. Note that two microphases

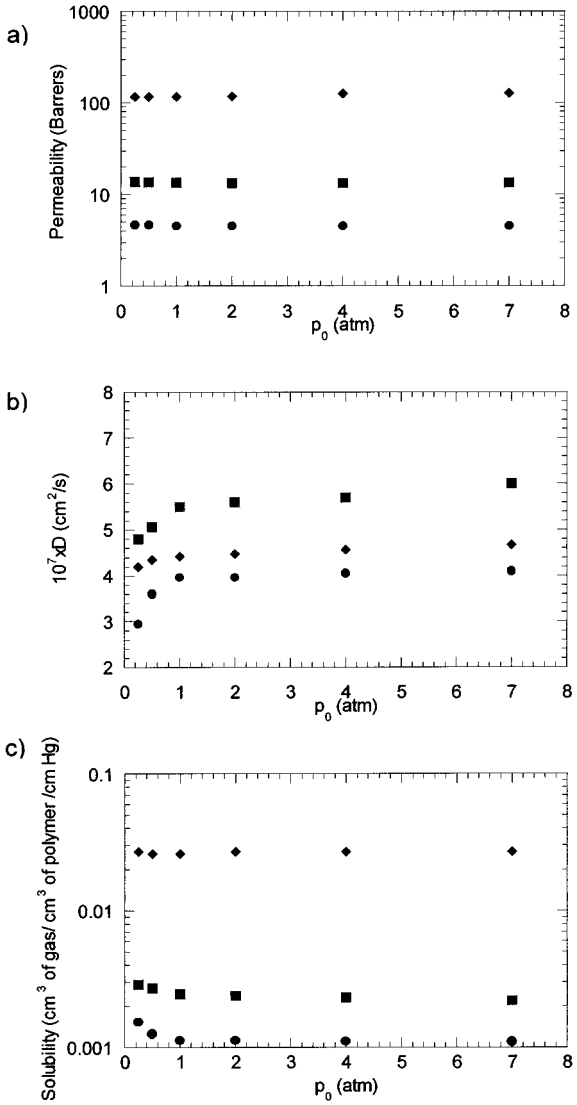

Figure 6. Variation of the apparent permeability (a), diffusion (b), and solubility (c) coefficients of CO_2 (◆), O_2 (■), and N_2 (●) with the pressure of the upstream chamber at 25 °C in PAALA-6 films.

(polypeptide helices and alkyl side chains) are present in PAALA-6 and that this microheterogeneity may be the responsible for such changes.

On the assumption that the films are homogeneous systems, the transport of gases through the films may be described as a thermally activated process where the temperature dependence of the permeability parameters obeys the Arrhenius law given by

$$X = X_0 \exp\left(-\frac{E_x}{RT}\right) \tag{8}$$

In this equation, X stands for either the permeability or the diffusion coefficient, whereas X_0 and E_x are their corresponding preexponential factors and activation energies, respectively. Activation energies associated with the diffusion process may be therefore determined from semilogarithmic plots of X against $1/T$, as depicted in Figure 7. The values of E_P and E_D obtained by this means are compared in Table 3. It can be seen that the relative values of E_P and E_D follow the trends $E_P(CO_2) < E_P(N_2) < E_P(O_2)$ and $E_D(CO_2) > E_D(O_2) > E_D(N_2)$ and that E_P is smaller than E_D for all cases. Consequently,

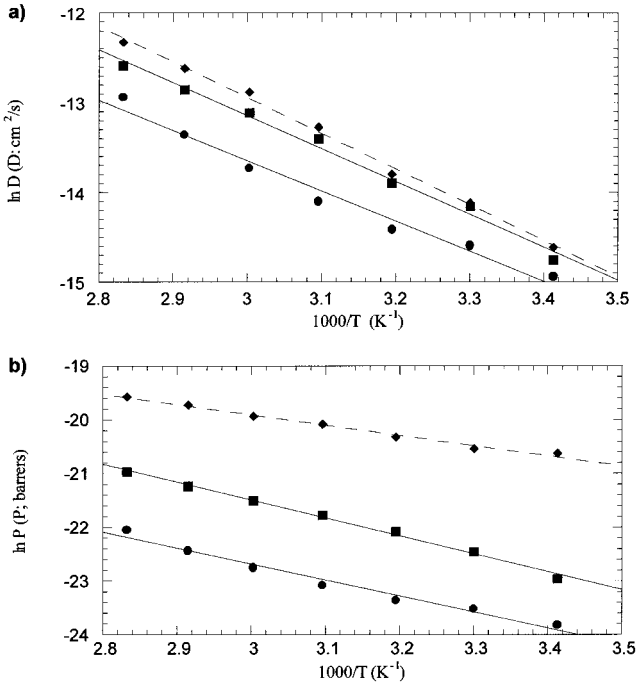

Figure 7. Arrhenius plots for the apparent diffusion (a) and permeability (b) coefficients of CO_2 (◆), O_2 (■), and N_2 (●). The values were obtained at 25 °C under an upstream pressure of 1 atm.

Table 3. Activation Energy (kcal/mol) for CO_2, O_2, and N_2 Obtained from Permeabilities and Diffusion Coefficient Measurements through PAALA-6 Films

gas	E_P (kcal mol^{-1})	E_D (kcal mol^{-1})	ΔH_S (kcal mol^{-1})[a]
CO_2	3.9	8.0	−4.1
O_2	6.6	7.4	−0.8
N_2	6.0	6.7	−0.7

[a] Heat of solution $\Delta H = (E_P - E_D)$.

Table 4. Permselectivity of PAALA-6 Films

T (°C)	$P(CO_2)/P(O_2)$	$P(CO_2)/P(N_2)$
20	10.3	24.4
30	6.8	22.7
40	5.8	21.1
50	5.4	20.2
60	4.8	16.8
70	4.6	15.1
80	4.0	12.0

the heat of solution, ΔH_s, of PAALA-6 is negative and decreases from N_2 to CO_2 in a similar manner as happens in other polymers such as stretched films of linear low-density polyethylene films prepared from copolymers of ethylene-1-octene.[31]

The permselectivity of films is usually expressed in terms of an ideal separation factor, $\alpha(A/B)$, equal to the ratio of the permeability coefficient of the two gases considered.

$$\alpha\left(\frac{A}{B}\right) = \frac{P_A}{P_B} = \frac{D_A}{D_B}\frac{S_A}{S_B} \tag{9}$$

Accordingly, values of the selectivity coefficient of CO_2 respect to N_2 and O_2 resulting for PAALA-6 used in this study are shown in Table 4, which shows that the transport of CO_2 is favored respect to both N_2 and O_2. As expected, an increase in temperature tends to decrease the permselectivity of the films.

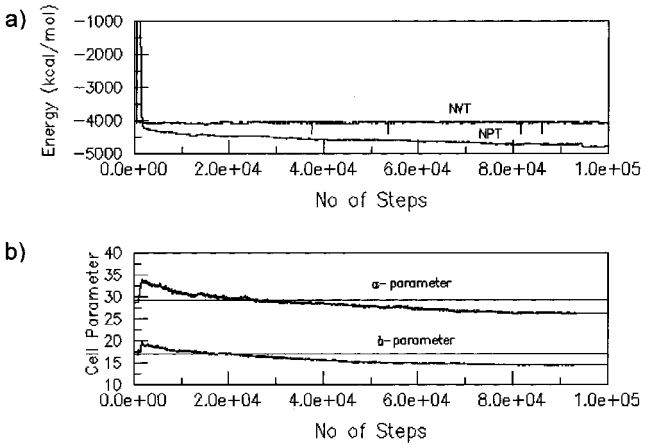

Figure 8. (a) Energy of PAALA-6 provided by MC/1 and MC/2 simulations as a function of the number of steps. (b) Cell parameters of PAALA-6 provided by MC/2 simulation as a function of the number of steps.

Computer Simulations. The Structure of PAALA-6 Revisited. The poorly ordered nature of PAALA-6 makes difficult the structural study of this polymer by X-ray diffraction.[5,6] The scarce number of reflections observed in the diffraction patterns are broad and diffuse, adding a considerable degree of uncertainty to spacing determinations. For this reason, the so-called hexagonal form of PAALA-*n* common to members with $n \leq 4$ was used as a model to interpret the structure of PAALA-6. The crystal unit cell of such a form is monoclinic with two chains in antiparallel arrangement although for simplicity it is usually described in terms of a hexagonal pseudocell containing only one chain. Thus, PAALA-6 was assumed to consist of a roughly hexagonal packing of right-handed 13/4 helices with an approximate interchain distance of 17 Å.[6] Since the size of hexyl side chains is unsuitable to pack efficiently in a three-dimensional crystal array, the helices should be staggered at random. An atomistic description of this structure was provided some years ago using simple energy minimization techniques with the lattice parameters inferred from X-ray diffraction data. As we will see below, large discrepancies between experimental and calculated solubility coefficients were obtained when such a structure was used for simulation. To get a more accurate description of the crystal structure of PAALA-6 which could explain better experimental permeation results, we ran two MC simulations at room temperature. The first one (MC/1) was performed under *NVT* conditions using the lattice parameters estimated from experimental data corresponding to a rectangular lattice of $a = 17.0$ Å and $b = 29.4$ Å.[6] In the second simulation (MC/2), which was of *NPT* type, the dimensions of the box were initially set as indicated in the Methods section and allowed to vary. In both cases, the *c* parameter of the lattice was kept 19.9 Å, which is the length of the identity period of the 13/4 helix of PAALA-*n*.

Figure 8a shows the evolution of the energy as a function of the number of steps for both MC/1 and MC/2. It can be seen that the system was equilibrated rapidly in the two cases, but the structure resulting from the MC/2 simulation became more stable than that resulting from MC/1. Figure 8b shows the evolution of the lattice parameters *a* and *b* along the MC/2 simulation. Both parameters, *a* and *b*, were found to shorten spontaneously with relative changes of about 15 and 10%, respectively. Thus, MC/2 simulations predict a quasi-hexagonal pseudocell for PAALA-6 with parameters smaller than those provided by energy minimization methods. The density calculated for this highly compacted structure is 1.12 g mL^{-1}, in much better agreement with the measured value (1.07 g mL^{-1}) than that calculated for the structure resulting from MC/1 simulation, which is 0.86 g mL^{-1}.

Inspection of the side chain dihedral angles of the different molecules contained in the simulation boxes of either MC/1 or MC/2 corroborates that the hexyl group is not crystallized. Thus, equivalent residues belonging to independent molecules show quite different conformational angle distributions. This is illustrated in Figure 9a, which displays the conformational distribution of the two central dihedral angles for the sixth residue of the four molecules pointing to the same directions (empty circles in the simulation box depicted in Figure 3). It should be mentioned that for a three-dimensional ordered arrangement the conformation distributions should be identical or almost identical. Similar results were obtained when other residues were analyzed (data not shown). On the other hand, the helices become slightly tilted with respect to the *c*-axis of the structure, an effect that had been previously detected with higher intensity by energy minimization calculations.[6] Figure 9b shows a representative structure of PAALA-6 as projected along the *c*-axis with 13/4 helices hexagonally packed and the hexyl side chains in the liquid state. In conclusion, the MC simulations carried out in this study reveal that the structure of PAALA-6 should be more compacted than previously described and corroborate that the hexyl side chains are in the liquidlike state.

Predicted Solubilities. MC simulations of *NVT* type were performed in order to compute the solubilities of N_2, O_2, and CO_2 in PAALA-6 at room temperature. Calculations were performed at 20 °C using the parameters for the uncompacted (MC/3 simulation) and compacted (MC/4 simulation) lattices described in the previous section. Both simulations were run for a total of 1×10^6 steps. The starting structures of MC/3 and MC/4 were the last snapshot provided by MC/1 and MC/2, respectively, and therefore no equilibration period was required. Indeed, MC/3 is only an enlargement of MC/1. It should be noted that in order to apply the Widom's test-particle insertion method, the volume of the simulation box is convenient to be kept constant.

As a first step, we examined the unoccupied space for all the generated microstructures. The results are summarized for each penetrant in Table 5, which displays the amount of unoccupied space averaged over the 200 microstructures recorded from MC/3 and MC/4 simulations. It should be noted that the amount of unoccupied space has been used by a number of authors to interpret a variety of polymer properties.[32−34] As expected, the available space calculated by MC/4 is smaller than that obtained by MC/3. Furthermore, in the former case, the amount of unoccupied space is similar for the three penetrants, whereas MC/4 simulations yield a significantly higher value for CO_2. Figure 10 illustrates the amount and distribution of the unoccupied space for CO_2 in representative structures of PAALA-6 generated by MC/3 and MC/4. On the other hand, it is striking that the unoccupied space for O_2 and N_2 becomes reduced up to 20 times when the compacted lattice, whose volume is only 80% of the uncompacted

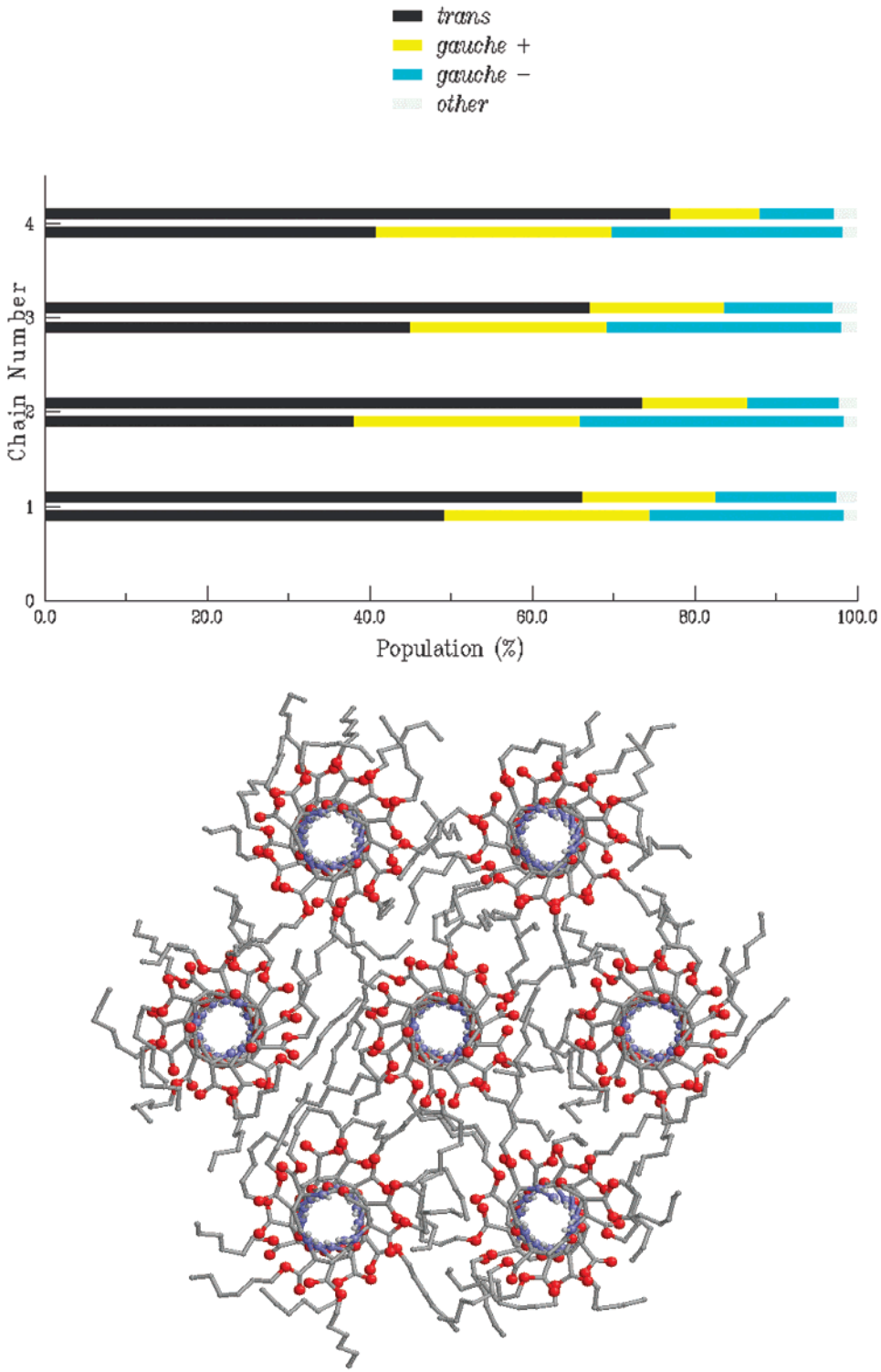

Figure 9. (a) Conformational distribution obtained from MC/2 for two consecutive side chain dihedral angles of the sixth residue of the four independent chains arranged in the same direction (see Figure 3). (b) Projection along the *c*-axis of a representative snapshot obtained from MC/2 simulation. Note that the helices are slighted twisted with respect to the *c*-axis.

one, is used for calculations. Such dramatic change in the available space may be accounted by a "densification" process that takes place when the interchain distances are too large. In this situation the void volume is distributed in large cavities that are very efficient in accommodating the penetrants. When the chains close up to each other at the equilibrium distances, the space is evenly distributed in small cavities, many of then being too small as to be occupied by the penetrants. This restriction is more severe for the case of spherical particles (O_2 and N_2) with regards to ellipsoids (CO_2) since the anisometry of these particles allows a more efficient accommodation in the elongated space provided by the cavities.

Table 6 shows the calculated excess chemical potentials for the three penetrants investigated. The predicted solubilities, which were calculated using eqs 1 and 2, are compared with the experimental data in the same table. For both MC/3 and MC/4, the calculated solubility increased in the order $CO_2 > O_2 > N_2$, according to what

Table 5. Predicted Unoccupied Space[a] (%) for Penetrants in the Quasi-Hexagonal Structure of PAALA-6

lattice[b]	simulation	T (°C)	O_2	N_2	CO_2
a = 17.0 Å, b = 29.4 Å, c = 19.9 Å	MC/3	20	2.39	2.07	2.36
a = 14.6 Å, b = 26.4 Å, c = 19.9 Å	MC/4	20	0.13	0.10	0.70
	MC/5	80	0.34	0.26	0.19

[a] Unoccupied space has been computed considering different temperatures and different simulation boxes and averaged over the 200 microstructures generated by MC simulations of *NVT* type. [b] Models built using the lattice parameters obtained from energy minimization[6] and MC simulation methods.

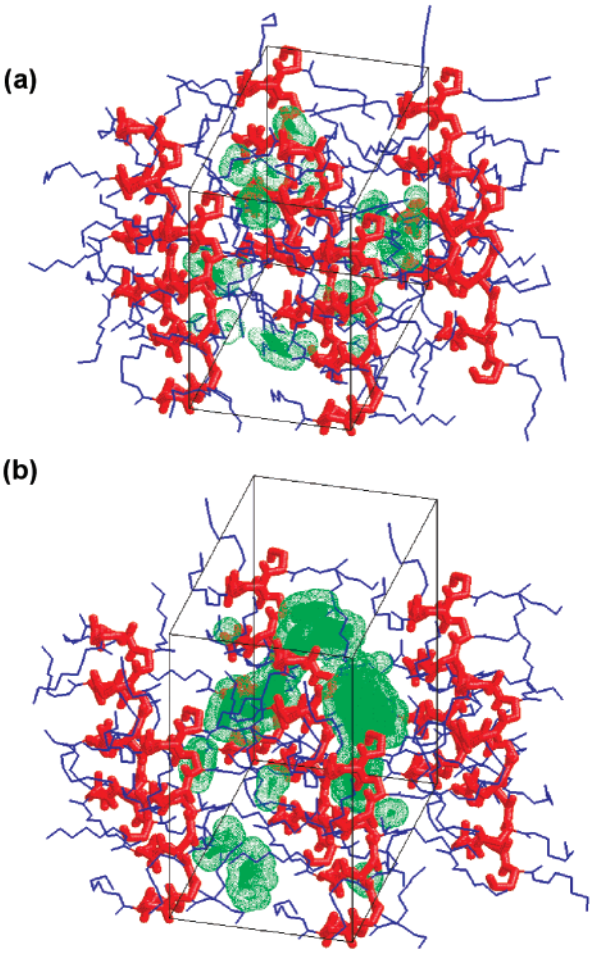

Figure 10. Unoccupied space for CO_2 in one of the microstructures of PAALA-6 generated by MC/3 (a) and MC/4 (b).

is experimentally observed. However, a quantitative comparison of calculated and experimental data reveals a strong discrepancy between MC/3 and MC/4. The solubilities predicted by MC/3 are overestimated by almost 2 orders of magnitude with respect to those obtained from experimental P and D values by means of eq 7. Conversely, the solubilities predicted by MC/4 are comparable to those derived from experimentation, the calculated values being around 3 times higher than the experimental ones. It should be noted that the value of S depends on the accuracy of P and D and that these coefficients are largely determined by the crystallinity of the sample. Unfortunately, the latter effect has not been considered in our computational simulations. At any case, comparison of results obtained with MC/3 and MC/4 clearly indicates that the lattice parameters resulting from *NPT* simulations provide a more correct description of the structure of PAALA-6 than was previously attained.

Finally, we have investigated the effect of the temperature on the predicted solubilities by MC simulations. For this purpose, we run MC simulations of *NVT* type at 80 °C (MC/5). The unoccupied spaces, excess chemical potential, and calculated solubility for the three penetrants are included in Tables 5 and 6. Results indicate that the amount of unoccupied space for spherical penetrants increases with the temperature. Thus, the space available for the O_2 and N_2 penetrants is close to 3 times larger at 80 °C than at 20 °C, and the predicted solubilities are therefore between 2 and 3 times greater. This is poor agreement with experimental data, which show that the solubilities of O_2 and N_2 are almost independent of the temperature. An opposite behavior is simulated for CO_2. The available space for this penetrant was found to decrease more than 3 times when the temperature increased from 20 to 80 °C, and as a consequence, the solubility predicted at 80 °C for CO_2 in PAALA-6 arrives to be about 7 times smaller than that calculated at 25 °C. This trend is in accordance with experimental results which show that the solubility of CO_2 in PAALA-6 decreases about 3 times when the temperature rises. Calculations at 80 °C using the uncompacted lattice (data not shown) showed the same trend for the three gases. At this moment we have not a plausible explanation for the lack of concordance found for the spherical penetrants N_2 and O_2. It is clear, however, that the redistribution of the interatomic space that takes place upon heating is defectively simulated.

We might summarize the discussion of the computer simulations by noting that the estimates of the solubility coefficients provided at room temperature by the theoretical strategy employed in this work are in good agreement with experimental values. Not only the predicted and experimental parameters are of the same order of magnitude, but the differences in solubilities between different polymers are also reproduced. The goodness of these computational results is probably due to the accurate description of the structural behavior of PAALA-6 provided by the MC simulations. Unfortunately, simulations at high temperatures produces

Table 6. Calculated Excess Chemical Potentials (μ_{ex}, in kcal mol^{-1}), Predicted Solubilities (S_{calc}, in barrers), and Experimental Solubilities (S_{exp}, in barrers) for Penetrants in the Quasi-Hexagonal Structure of PAALA-6

lattice	simulation	T (°C)		O_2	N_2	CO_2
a = 17.0 Å, b = 29.4 Å, c = 19.9 Å	MC/3	25	μ_{ex}	−1.34	−1.25	−2.01
			S_{calc}	11×10^{-2}	9.8×10^{-2}	35×10^{-2}
			S_{exp}	0.27×10^{-2}	0.14×10^{-2}	2.4×10^{-2}
a = 14.6 Å, b = 26.4 Å, c = 19.9 Å	MC/4	25	μ_{ex}	0.40	0.57	−1.15
			S_{calc}	0.60×10^{-2}	0.50×10^{-2}	8.3×10^{-2}
			S_{exp}	0.27×10^{-2}	0.14×10^{-2}	2.4×10^{-2}
a = 14.6 Å, b = 26.4 Å, c = 19.9 Å	MC/5	80	μ_{ex}	−0.16	−0.02	−0.20
			S_{calc}	1.5×10^{-2}	1.2×10^{-2}	1.2×10^{-2}
			S_{exp}	0.23×10^{-2}	0.11×10^{-2}	0.72×10^{-2}

unsatisfactory results most probably due to the inefficiency of the method to evaluate the changes in shape of the cavities that take place upon heating. Further improvements of the methodology taking into account temperature effects on the distribution of the void space are required, research which is underway in our laboratory.

Acknowledgment. This research has been supported by Ministerio de Ciencia y Tecnología (Grants BQU2000-0990) and by Fundació Caixa-Castelló through Grant P1B97-03. The authors are indebted to CESCA for computational facilities. David Zanuy acknowledges the grant received from the Ministerio de Educación to support the realization of his PhD.

References and Notes

(1) Muñoz-Guerra, S.; López-Carrasquero, F.; Fernández-Santín, J. M.; Muñoz-Guerra, S. In *Polymeric Materials Encyclopedia*; Salamone, J. C., Ed.; CRC Press: Boca Raton, FL, 1996; Vol. 6, p 4694.
(2) López-Carrasquero, F.; García-Alvarez, M.; Muñoz-Guerra, S. *Polymer* **1994**, *35*, 4502.
(3) López-Carrasquero, F.; García-Alvarez, M.; Navas, J. J.; Alemán, C.; Muñoz-Guerra, S. *Macromolecules* **1996**, *29*, 8449.
(4) López-Carrasquero, F.; Alemán, C.; García-Alvarez, M.; Martínez de Ilarduya, A.; Muñoz-Guerra, S. *Macromol. Chem. Phys.* **1995**, *196*, 253.
(5) López-Carrasquero, F.; Montserrat, S.; Martínez de Ilarduya, A.; Muñoz-Guerra, S. *Macromolecules* **1995**, *28*, 5535.
(6) Navas, J. J.; Alemán, C.; López-Carrasquero, F.; Muñoz-Guerra, S. *Polymer* **1997**, *38*, 3484.
(7) Zanuy, D.; Alemán, C.; Muñoz-Guerra, S., submitted.
(8) Puleo, A. C.; Paul, D. R.; Wong, P. K. *Polymer* **1989**, *30*, 1357.
(9) Mohr, J. M.; Paul, D. R. *Polymer* **1991**, *32*, 1236.
(10) Durrill, P. L.; Griskey, R. G. *AIChE J.* **1996**, *15*, 106.
(11) Mogri, Z.; Paul, D. R. *Polymer* **2001**, *42*, 2531.
(12) Zanuy, D.; León, S.; Alemán, C.; Muñoz-Guerra, S. *Polymer* **2000**, *41*, 4169.
(13) Zanuy, D.; Namba, A.; León, S.; Alemán, C.; Muñoz-Guerra, S. *Polymer* **2001**, *42*, 281.
(14) Zanuy, D.; Alemán, C.; López-Carrasquero, F.; Báez, M. E.; García-Alvarez, M.; Laso, M.; Muñoz-Guerra, S. *Macromol. Chem. Phys.* **2001**, *202*, 564.
(15) Loos, K.; Muñoz-Guerra, S. In *Supramolecular Polymers*; Ciferri, A., Ed.; Marcel Dekker: New York, 2000.
(16) Rodríguez-Galán, A.; Muñoz-Guerra, S.; Subirana, J. A.; Chuong, B.; Sekiguchi, H. *Makromol. Chem., Macromol. Symp.* **1986**, *6*, 277.
(17) García-Alvarez, M.; López-Carrasquero, F.; Tort, E.; Rodríguez-Galán, A.; Muñoz-Guerra, S. *Synth. Commun.* **1994**, *24*, 745.
(18) Tanaka, S. Ph.D. Thesis, University of Kyoto, 1972.
(19) De Pablo, J. J.; Laso, M.; Suter, U. W. *J. Chem. Phys.* **1992**, *96*, 6157.
(20) Siepmann, J. I.; Frenkel, D. *Mol. Phys.* **1992**, *75*, 59.
(21) León, S.; Alemán, C.; Escalé, F.; Laso, M. *J. Comput. Chem.* **2001**, *22*, 162.
(22) Martínez de Ilarduya, A.; García-Alvarez, M.; Alemán, C.; López-Carrasquero, F.; Muñoz-Guerra, S. *Macromolecules* **1999**, *32*, 3257.
(23) Weiner, S. J.; Kollman, P. A.; Case, D. A.; Singh, U. C.; Ghio, C.; Alagona, G.; Profeta, S.; Weiner, P. *J. Am. Chem. Soc.* **1984**, *106*, 765.
(24) Müller-Plathe, F. *Macromolecules* **1991**, *24*, 6475.
(25) Widom, B. *J. Phys. Chem.* **1982**, *86*, 869.
(26) Barrer, R. M. *Trans Faraday Soc.* **1939**, *35*, 628.
(27) Compañ, V.; López-Lidón, M.; Andrio, A.; Riande, E. *Macromolecules* **1998**, *31*, 6984.
(28) Glatz, F. P.; Mülhanpt, R. *J. Membr. Sci.* **1991**, *90*, 151.
(29) Haraya, K.; Hwang, S. T. *J. Membr. Sci.* **1992**, *71*, 13.
(30) Michaels, A. S.; Bixler, H. *J. Polym. Sci.* **1961**, *50*, 393.
(31) García-Villaluenga, J. P.; Seoane, B.; Compañ, V.; Diaz-Calleja, R. *Polymer* **1997**, *38*, 3827.
(32) Misra, S.; Mattice, W. L. *Macromolecules* **1993**, *26*, 7274.
(33) Arizzi, S.; Mott, P. H.; Suter, U. W. *J. Polym. Sci., Part B: Polym. Phys.* **1992**, *30*, 415.
(34) Shah, V. M.; Stern, S. A.; Ludovice, P. J. *Macromolecules* **1989**, *12*, 4660.

MA010321A